

We are IntechOpen, the world's leading publisher of Open Access books Built by scientists, for scientists

6,900

Open access books available

186,000

International authors and editors

200M

Downloads

Our authors are among the

154

Countries delivered to

TOP 1%

most cited scientists

12.2%

Contributors from top 500 universities



WEB OF SCIENCE™

Selection of our books indexed in the Book Citation Index
in Web of Science™ Core Collection (BKCI)

Interested in publishing with us?
Contact book.department@intechopen.com

Numbers displayed above are based on latest data collected.
For more information visit www.intechopen.com



Study on the Mechanism of Traumatic Brain Injury

Yuelin Zhang¹, Shigeru Aomura²,
Hiromichi Nakadate² and Satoshi Fujiwara³

¹*Tokyo University of Agriculture and Technology,*

²*Tokyo Metropolitan University,*

³*Yokohama City University,*

Japan

1. Introduction

Skull fracture, intracranial hemorrhage, or cerebral injury can be caused in humans due to a strong impact to the head. The following 2 types of cerebral injuries are often observed: one type is cerebral contusion which is a local brain damage to the brain, and the other is diffuse axonal injury (DAI) which is a diffuse brain damage to the brain. In various head injuries caused by external impact, cerebral contusion and DAI mainly result in direct failure of the cerebral parenchyma.

Cerebral contusions can be either coup or contrecoup contusions that occur on either the same or the opposite side of impact, respectively (Yanagida et al., 1989). Cerebral contusions are caused by rapid pressure fluctuations transmitted to the brain surface via the cerebrospinal fluid (CSF) (Fujiwara et al., 1989, Zhang et al., 2001). The hypothesis that the brain surface is destroyed when the cerebral parenchyma collides with the skull, although intuitive, has never been observed (Gurdjian et al., 1966). The cavitation theory states that the pressure gradient generated in the CSF by impact causes contrecoup negative pressure on the opposite side of impact and forms cavitation bubbles; the subsequent collapse of the bubbles causes brain tissue damage. Although this theory can be trusted, no collapse of bubbles in the head has yet been observed (Gross, 1958). Although various theories report the generation mechanism of cerebral contusion, none can sufficiently explain the entire mechanism. For predicting the dynamic response of the human head, numerous cadaver and animal experiments have been performed (Nahum & Smith, 1977; Gennarelli, 1983); however, these experiments are difficult to conduct because of cost and/or ethical concerns. Furthermore, the finite element method is widely used to predict the dynamic responses of the human head (Aomura et al., 2002). Some researchers report the reconstruction of real-world brain injury cases using multibody dynamics and finite element method (Raul et al., 2006; Riordain et al., 2003; Doorly & Gilchrist, 2006). These studies demonstrate the effectiveness of these methods but do not explain the mechanism of the brain injuries themselves.

DAI is considered to be caused by strain to the brainstem due to the rotational movement of the head. When a human head receives an external impact, the cranium moves first and then the brain follows its movement; this delay becomes more remarkable inside the brain, and a large strain is generated in the deep brain. This large strain causes damage to the axons of nerve cells and results in DAI (Fujiwara et al., 1998; Ommaya & Gennarelli, 1974).

As described above, in the past few decades, in order to clarify the mechanism of cerebral contusion and DAI, the impact experiments using physical models and animals, numerical analysis by finite element method are performed as an engineering approach. In recent years, in order to clarify the tolerance of impact at the cellular level, the impact experiments are performed using cultured neuronal cells and tissues as a biological approach. However, these researches often focus on the mechanism of only one type of injury; can not evaluate all types of traumatic brain injury comprehensively. Thus, future research should be performed concurrently using engineering and biological approaches. Therefore, in this study, the reconstruction analyses of real-world brain injury accident cases are performed to understand the mechanism of cerebral contusion and the impact experiments of cultured cells are performed to understand the mechanism of DAI.

2. Finite-element human head model

A computer model was constructed using cross-sectional T1 weighted MRI data of a woman's head because it was recently decided that CT should not be used for research to avoid radiation exposure. The slice thickness of the data is 3.3mm, and the slice interval is 0.0mm. Both the internal and external boundary curves of the scalp, skull, CSF, brain, and brain stem were extracted by binary image processing of the MRI data to make the internal and external surfaces of each part of the model. Three-dimensional human head models with hexahedral elements were made between the internal and external surfaces of each part (Fig. 1). The three-layered structure of the skull, which consists of an outer table, diploe, and inner table, was also reproduced. Finally, the finite element model consisted of 147,723 nodes and 114,012 elements. The material properties of each part of the model are shown in Table 1 (Willinger & Baumgartner, 2003; Nishimoto et al., 1998; Viano et al., 1998). Elastic properties were assigned to the scalp (Willinger & Baumgartner, 2003) and skull (Nishimoto et al., 1998), and viscoelastic properties were assigned to the CSF, brain, and brain stem (Viano et al., 1998).

For verifying the finite element model, the numerical results were compared with those results of the cadaver experiment by Nahum (Nahum & Smith, 1977). The impact direction was along the specimen's mid-sagittal plane, and the head was rotated forward such that the Frankfort anatomical plane was inclined 45° from the horizontal plane. The outline of the experiment is shown in Fig. 2(a). In the experiment, a 5 kg iron impactor was impacted to the head at 6 m/s (used by Nahum). However, Nahum does not definitively show what types of padding materials were interposed between the skull and impactor; therefore, in numerical calculations of this study only the time-force history (Fig. 2(b)) was used as described in the literature (Nahum & Smith, 1977). The restraint condition of the head was free because the cadaver subject was seated and not restrained around the neck. The slide-type contact condition was used between the skull and CSF, CSF and brain, and brain and brain stem.

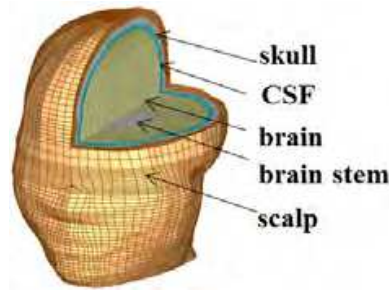
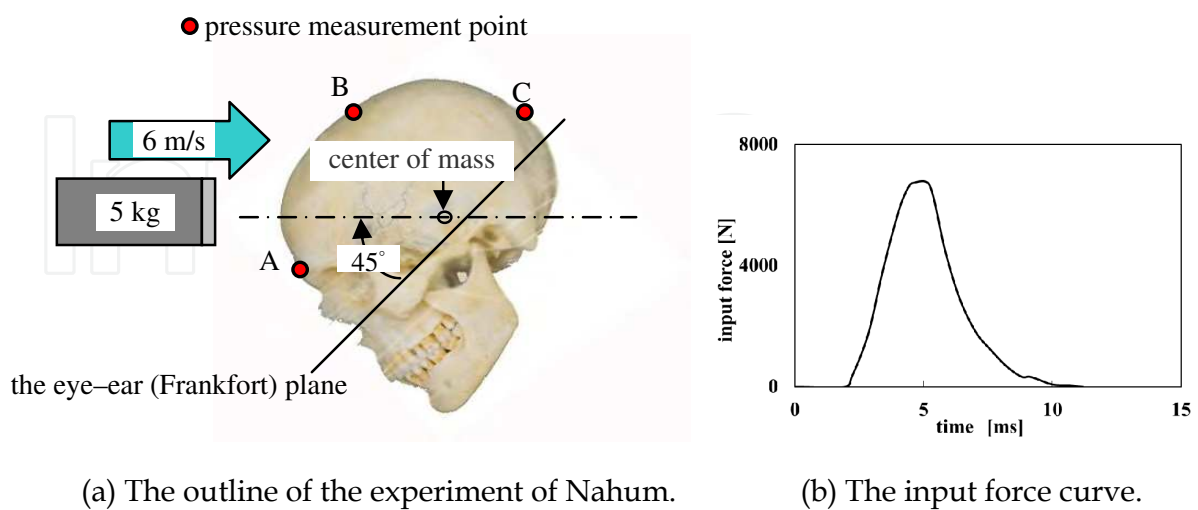


Fig. 1. Finite element human head model. The model consists of the scalp, skull (outer table, diploe, and inner table), CSF, brain, and brain stem.

	Scalp	Outer/inner table	Diploe	CSF	Brain	Brain stem
Density ρ (kg/m ³)	1000	1456	850	1040	1040	1040
Young's Modulus E (MPa)	16.7	8750	4660	-	-	-
Bulk Modulus K (MPa)	-	7120	3470	2190	2190	2190
Short Time Shear Modulus G ₀ (MPa)	-	-	-	-	0.0125	0.0225
Long Time Modulus G _∞ (MPa)	-	-	-	0.0005	0.0025	0.0045
Tangent Modulus (MPa)	-	4620	2170	-	-	-
Yield(MPa)	-	41.8	13.6	-	-	-
Poisson's Ratio ν (-)	0.42	0.25	0.25	-	-	-
Time Constant (1/s)	-	-	-	500000	80	80

Table 1. Material properties of the finite element human head model. Elastic properties were assigned to the scalp (Willinger & Baumgartner, 2003) and skull (Nishimoto et al., 1998), and viscoelastic properties were assigned to the CSF, brain, and brain stem (Viano et al., 1998).

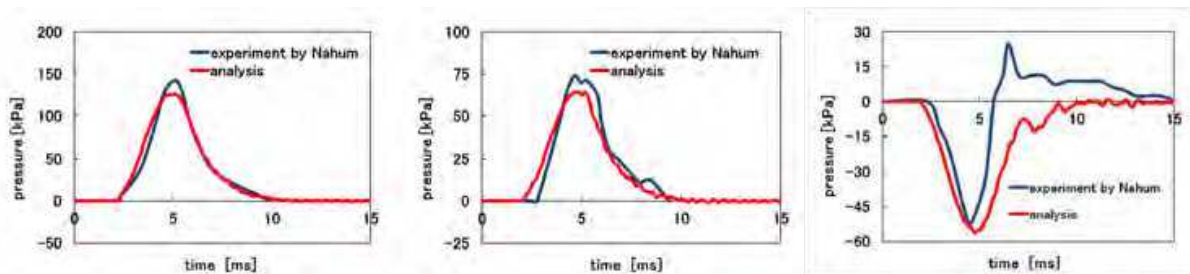
The experimental pressure response given by Nahum and pressure response calculated using finite element model in this study are shown in Fig. 3. Although slight difference was observed between the experimental and numerical results, this model was corroborated by the experimental cadaver test and sufficiently predicted intracranial pressure.



(a) The outline of the experiment of Nahum.

(b) The input force curve.

Fig. 2. Experiment by Nahum (Nahum & Smith, 1977). (a)The 5 kg iron impactor impacted the frontal region of the head at 6 m/s, and intracranial pressures were measured in the frontal (point A), parietal (point B) and occipital (point C) region of the head. (b) The input force curve obtained from the experiment.



(a) Frontal region(point A) (b) Parietal region(point B) (c) Occipital region(point C)

Fig. 3. Comparison to the cadaver experiment by Nahum (Nahum & Smith, 1977) and numerical calculation. The validation demonstrates that this model is corroborated by an experimental cadaver test and sufficiently predicts intracranial pressure.

3. The mechanism of cerebral contusion

Fujiwara et al. analyzed 105 real-world fatal brain injury cases (Fujiwara et al., 1986). Coup contusions are caused more easily by direct blows to the head than contrecoup contusions, and contrecoup contusions are caused more easily by falls and fall-downs than coup contusions (Fujiwara et al., 1986). In this study, input force duration which is strongly related to the impact region on the human head, impact velocity, stiffness, mass or shape of the impact object, was focused. Previous studies (Aomura et al., 2008; Zhang et al., 2010) using impact experiments and finite element analysis of a water-filled acrylic container have showed that negative pressure inside the container is caused by deformation of the acrylic wall; this negative pressure tends to occur on the impact side when the force duration is short and on the opposite side of impact when the force duration is long.

In this chapter, for understanding the relationship between input force duration and dynamic response inside the skull, 9 real-world brain injury accident cases, including 3 coup contusion cases and 6 contrecoup contusion cases, were simulated using a finite element human head model. Numerical calculations were performed using LS-DYNA version 971.

3.1 Real-world brain injury accident cases

The autopsy results (performed by S. Fujiwara), in which the cause of death was cerebral contusion, are shown in Table 2. In these cases, the type of impact was classified as a blow, fall, or fall-down. In each type of impact, the contusion was classified as a coup or contrecoup contusion. Coup contusions are predominant in blows, and contrecoup contusions are predominant in falls and fall-downs. According to the postmortem data in Table 2, coup contusions tend to occur due to impacts by sharp-cornered objects (cases 1–3), and contrecoup contusions, due to impacts by objects with flat surfaces (cases 4 and 5). Contrecoup contusions are predominant in all the cases of falls and fall-downs (cases 6–9). In the simulations, the pressure threshold for causing cerebral contusion was -100 kPa. Skull fracturing was also simulated, because it was observed in all cases. The tensile stress thresholds for causing skull fracture were 70.5 MPa for the outer and inner tables and 21.4 MPa for the diploe (Nishimoto et al., 1998).

Case	Impact object	Impact region	Fracture region	Contusion region	
				Coup	Contrecoup
1	Beer bottle	Frontal region	Frontal region	Lower side of frontal lobe	
2	Wooden box (1.5 t)	Right temporal region	Right temporal region ~ right cranial fossa (semi) crushing	Right parietal lobe	
3	Sake bottle (empty: 700g)	Right parietal region	Right parietal region	Right parietal lobe	
4	Tank lorry	Parieto-occipital region	Occipital region (crushing)		Lower side of left and right frontal lobes Lower side of left temporal lobe
5	Steel Box (600 kg)	Occipital region	Occipital region		Lower side of frontal lobe Right and left temporal lobe poles

(a) Blows. The data include 3 coup and 2 contrecoup contusions.

Case	Impact object (height/weight)	Impact region	Fracture region	Contusion region	
				Coup	Contrecoup
6	Concrete (5.5 m)	Upper side of occipital region	Occipital region		Lower side of frontal lobe
7	Wooden deck (10 m)	Occipital region	Occipital region		Lower side of frontal lobe Frontal pole

(b) Falls. The data include 2 contrecoup contusions.

Case	Impact object (height/weight)	Impact region	Fracture region	Contusion region	
				Coup	Contrecoup
8	Asphalt (160 cm/58 kg)	Occipital region	Occipital region		Frontal pole
9	Asphalt (156 cm/59 kg)	Right occipital region	Right temporal region		Lower side of right frontal lobe Lower side of right temporal lobe Lateral surface of left temporal lobe

(c) Fall-downs. The data include 2 contrecoup contusions.

Table 2. Postmortem data (cause of death was cerebral contusion, 1968~1984). In these cases, the type of impact was classified as a blow, fall, or fall-down. In each type of the impact, the contusion was classified as a coup or contrecoup contusion.

3.2 Simulations of real-world brain injury accident cases

In order to begin the simulation, the relative velocity between the head and impact object, and the impact position of each case must be estimated. In this study, the impact positions are described in the postmortem data (Table 2, Impact Region). The relative velocities between the head and impact objects were estimated in order to generate negative pressure in the lesion area of the brain and fracture the skull in the fracture region described in the postmortem data. The simulations of the 9 cases are shown below.

[Case 1]

The frontal region of the head was impacted by a beer bottle (467 g), causing a skull fracture at the frontal region and a coup contusion at the lower side of the frontal lobe. In the simulation, the impact velocity (1-15 m/s) was applied to the node that constituted the beer bottle model (Fig. 4(a)). In order to determine the impact velocity of this case, the following 2 conditions had to be satisfied:

1. The negative pressure must be generated on the impact side only, because a coup contusion was observed.
2. The frontal skull must be fractured.

The impact velocity that satisfies these conditions was around 10 m/s. The intracranial pressure fluctuations of the impact side and its opposite side are shown in Fig. 4(b). The input force duration (i.e. the length of time that the impact object contacted the head) of this case was counted from the animation of the analysis result, was 1.4 ms.

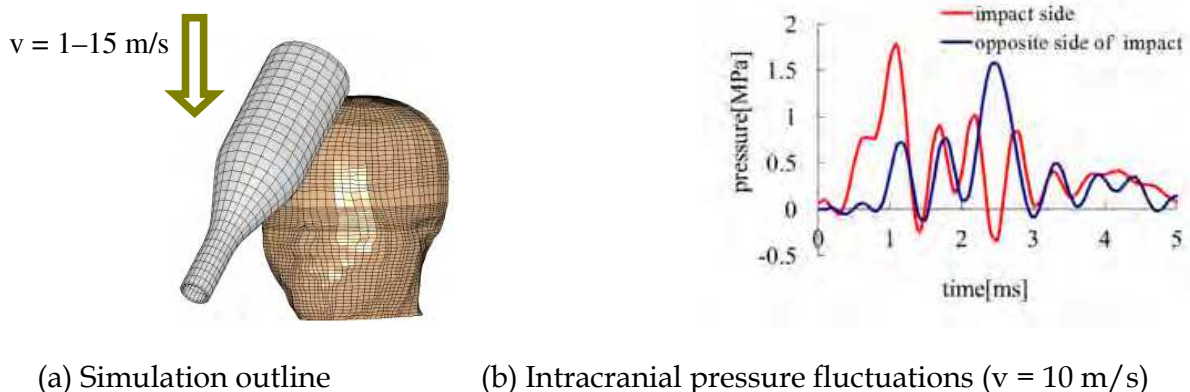


Fig. 4. Simulation outline and results of case 1. (a) Simulation outline. The impact velocity (1-15 m/s) was applied to the node that constituted the beer bottle model. (b) The intracranial pressure fluctuations of the impact side and its opposite side. The results show that negative pressure occurred only on the impact side.

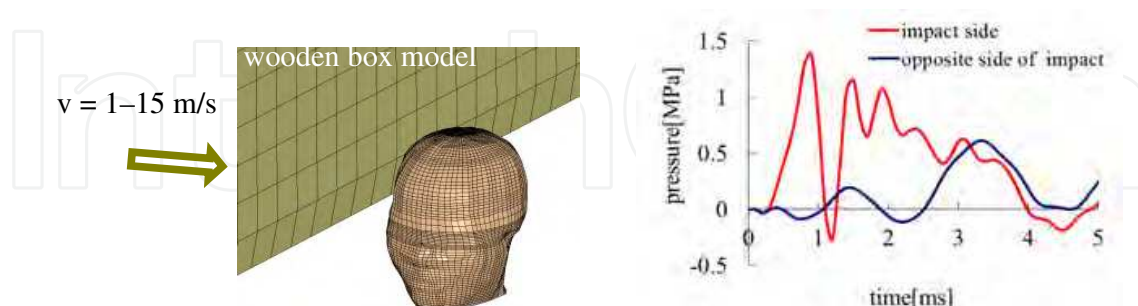
[Case 2]

The right temporal region of the head was impacted by a wooden box (1.5 t), causing a skull fracture from the right temporal region to the right cranial fossa and a coup contusion at the right parietal lobe. In the simulation, the impact velocity (1-15 m/s) was applied to the node that constituted the wooden box model (Fig. 5(a)). The impact velocity that satisfied this case was around 15 m/s, which caused negative pressure on the impact side (Fig. 5(b)) and skull fracture in the right temporal region of the head. The input force duration (i.e. the length of time that the impact object contacted the head) of this case was counted from the animation of the analysis result, was 2.7 ms.

[Case 3]

The right parietal region of the head was impacted by a sake bottle (700 g), causing a skull fracture at the right parietal region and a coup contusion at the right parietal lobe. In the simulation, the impact velocity (1-15 m/s) was applied to the node that constituted the sake

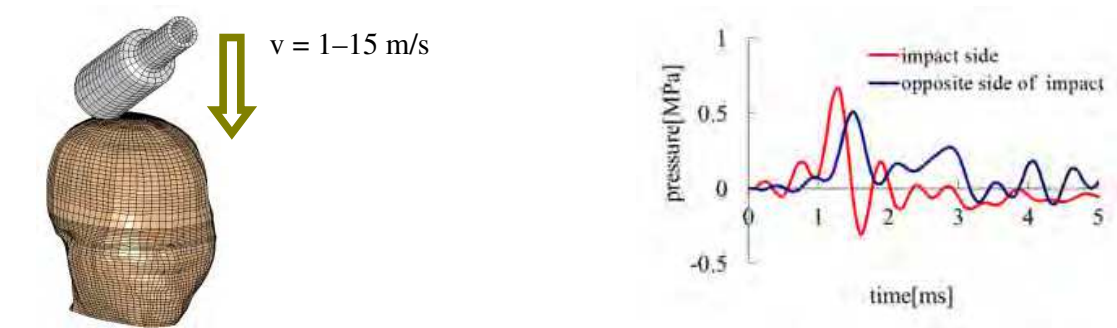
bottle model (Fig. 6(a)). The impact velocity that satisfied this case was around 15m/s, which caused the negative pressure at the impact side (Fig.6(b)) and the skull fracture at the right parietal of the head. The input force duration (i.e. the length of time that the impact object contacted the head) of this case was counted from the animation of the analysis result, was 2.2 ms.



(a) Simulation outline

(b) Intracranial pressure fluctuations ($v = 15 \text{ m/s}$)

Fig. 5. Simulation outline and results of case 2. (a) Simulation outline. The impact velocity (1-15 m/s) was applied to the node that constituted the wooden box model. For better view, only part of the wooden box is displayed. (b) The intracranial pressure fluctuations of the impact side and its opposite side. The results show that negative pressure occurred only on the impact side.



(a) Simulation outline

(b) Intracranial pressure fluctuations ($v = 15 \text{ m/s}$)

Fig. 6. Simulation outline and results of case 3. (a) Simulation outline. The impact velocity (1-15 m/s) was applied to the node that constituted the sake bottle model. (b) The intracranial pressure fluctuations of the impact side and its opposite side. The results show that negative pressure occurred only on the impact side.

[Case 4]

A man who was walking along the street was impacted by a tank lorry (6 t) at the parieto-occipital region of the head, causing a skull fracture at the occiput region and contrecoup contusions at the lower side of the left and right frontal lobes and in the lower side of left temporal lobe. In the simulation, the impact velocity (1-15 m/s) was applied to the node which constituted the tank lorry model (Fig.7(a)). The impact velocity which satisfied this case was around 10m/s, which caused the negative pressure at the opposite side of impact (Fig.7(b)) and the skull fracture at the occiput region of the head. The input force duration

(i.e. the length of time that the impact object contacted the head) of this case was counted from the animation of the analysis result, was 3.7 ms.

[Case 5]

A man who was working at a construction yard was impacted by a steel trash box (600 kg) at the occipital region of the head, causing a skull fracture at the occipital region and contrecoup contusions in the lower side of the frontal lobe and the right and left temporal lobe poles. In the simulation, the impact velocity (1–15 m/s) was applied to the node which constituted the steel box model (Fig.8(a)). The impact velocity which satisfied this case was around 9.5m/s, which caused the negative pressure at the opposite side of impact (Fig.8(b)) and the skull fracture at the occipital region of the head. The input force duration (i.e. the length of time that the impact object contacted the head) of this case was counted from the animation of the analysis result, was 3.6 ms.

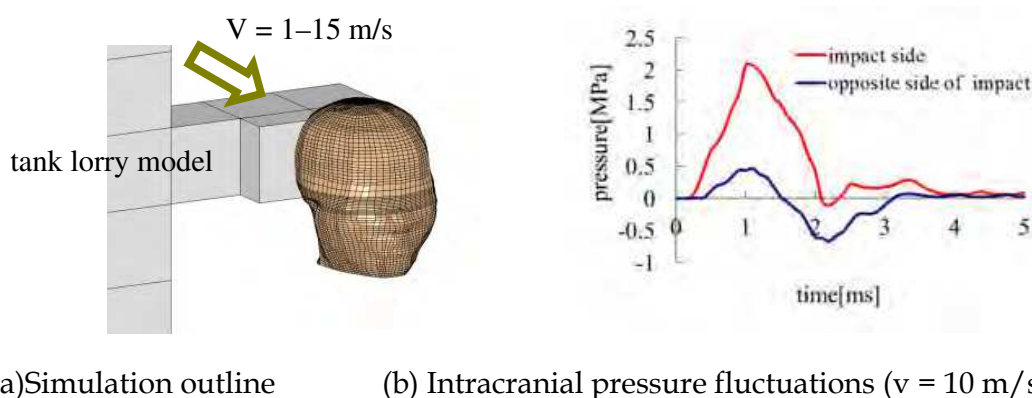


Fig. 7. Simulation outline and results of case 4. (a) Simulation outline. The impact velocity (1–15 m/s) was applied to the node that constituted the tank lorry model. For better view, only part of the tank lorry is displayed. (b) The intracranial pressure fluctuations of the impact side and its opposite side. The results show that negative pressure occurred only on the opposite side of impact.

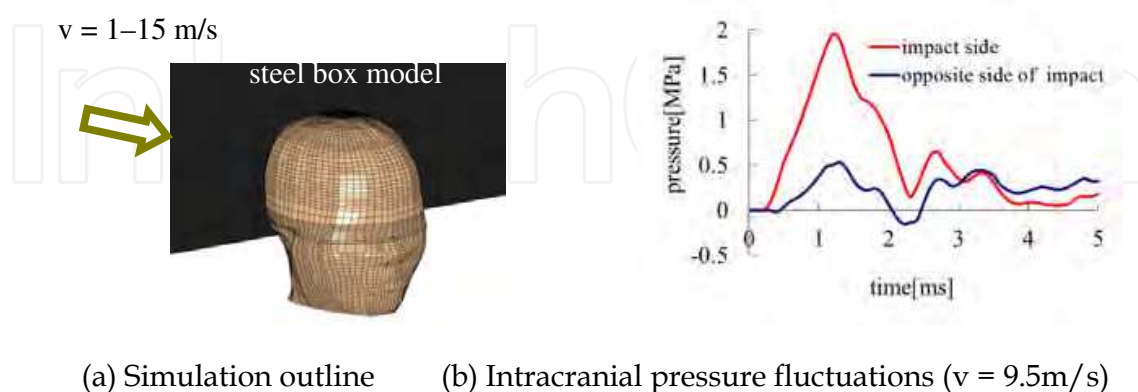
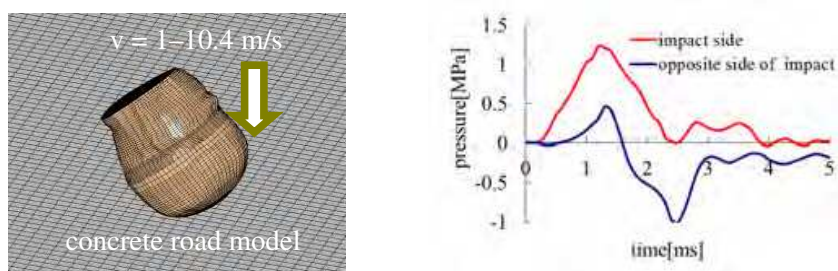


Fig. 8. Simulation outline and results of case 5. (a) Simulation outline. The impact velocity (1–15 m/s) was applied to the node that constituted the steel box model. For better view, only part of the steel box is displayed. (b) The intracranial pressure fluctuations of the impact side and its opposite side. The results show that negative pressure occurred only on the opposite side of impact.

[Case 6]

A man fell from 5.5 m high onto a concrete road, and the upper side of the occipital region of the head was impacted, causing a skull fracture at the occiput region and a contrecoup contusion at the lower side of the frontal lobe. In the simulation, the impact velocity (1–10.4 m/s, from the law of conservation of mechanical energy, the maximum velocity was calculated to be 10.4 m/s) was applied to the node that constituted the head model (Fig.9(a)). The impact velocity that satisfied this case was 10.4 m/s, which caused negative pressure on the opposite side of impact (Fig.9(b)) and a skull fracture in the occiput region of the head. The input force duration (i.e. the length of time that the impact object contacted the head) of this case was counted from the animation of the analysis result, was 3.7 ms.



(a) Simulation outline (b) Intracranial pressure fluctuations ($v = 10.4$ m/s)

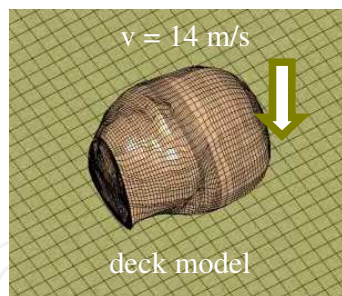
Fig. 9. Simulation outline and results of case 6. (a) Simulation outline. The impact velocity (1–10.4 m/s) was applied to the node that constituted the head model. For better view, only part of the concrete road model is displayed. (b) The intracranial pressure fluctuations of the impact side and its opposite side. The results show that negative pressure occurred only on the opposite side of impact.

[Case 7]

A sailor fell from 10 m high onto a deck, and the occipital region of head was impacted, causing a skull fracture in the occiput region and contrecoup contusions in the lower side of the frontal lobe and frontal pole. In the simulation, the impact velocity (1–14m/s, from the law of conservation of mechanical energy, the maximum velocity was calculated to be 14 m/s) was applied to the node that constituted the head model (Fig.10(a)). The impact velocity that satisfied this case was around 10 m/s, which caused negative pressure on the opposite side of impact (Fig.10(b)) and skull fracture in the occiput region of the head. The input force duration (i.e. the length of time that the impact object contacted the head) of this case was counted from the animation of the analysis result, was 3.6 ms.

[Case 8]

A man fell down onto an asphalt road, and the occipital region of the head was impacted, causing a skull fracture in the occiput region and a contrecoup contusion in the frontal pole. In the simulation, the impact velocity (1–15 m/s) was applied to the node which constituted the head model (Fig.11(a)). The impact velocity which satisfied this case was around 11m/s, which caused the negative pressure at the opposite side of impact (Fig.11(b)) and the skull fracture at the occiput region of the head. The input force duration (i.e. the length of time that the impact object contacted the head) of this case was counted from the animation of the analysis result, was 2.9 ms.



(a) Simulation outline

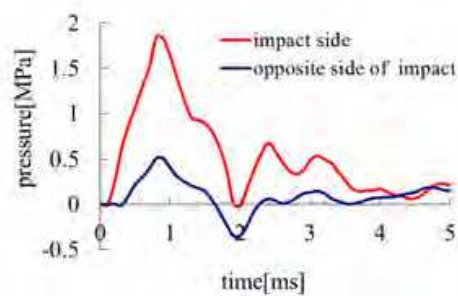
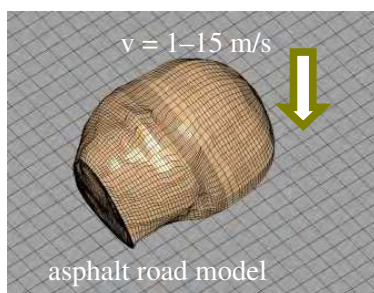
(b) Intracranial pressure fluctuations ($v = 10$ m/s)

Fig. 10. Simulation outline and results of case 7. (a) Simulation outline. The impact velocity (1-14 m/s) was applied to the node that constituted the head model. For better view, only part of the deck model is displayed. (b) The intracranial pressure fluctuations of the impact side and its opposite side. The results show that negative pressure occurred only on the opposite side of impact.



(a) Simulation outline

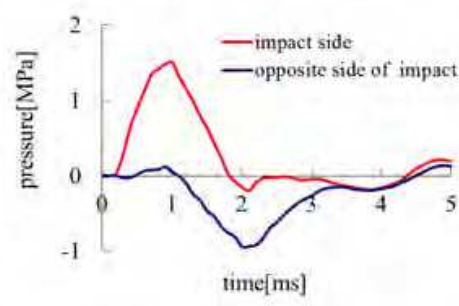
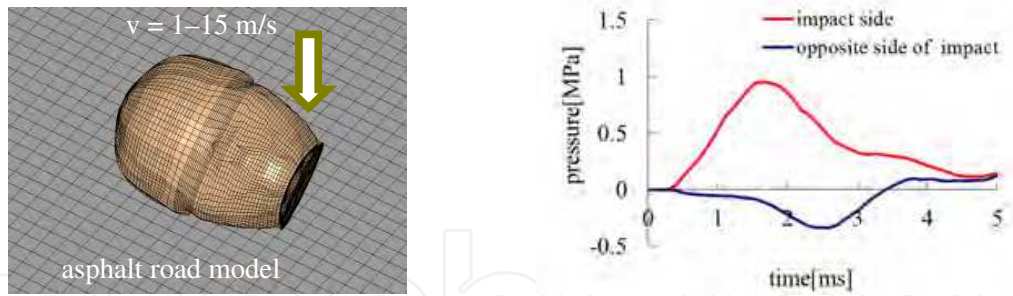
(b) Intracranial pressure fluctuations ($v = 11$ m/s)

Fig. 11. Simulation outline and results of case 8. (a) Simulation outline. The impact velocity (1-15 m/s) was applied to the node that constituted the head model. For better view, only part of the asphalt road model is displayed. (b) The intracranial pressure fluctuations of the impact side and its opposite side. The results show that negative pressure occurred only on the opposite side of impact.

[Case 9]

A man fell down onto an asphalt road, and the right occipital region of the head was impacted, causing a skull fracture in the right temporal region and contrecoup contusions in the lower sides of the right frontal and right temporal lobe and on the lateral surface of the left temporal lobe. In the simulation, the impact velocity (1-15 m/s) was applied to the node which constituted the head model (Fig.12(a)). The impact velocity which satisfied this case was around 7m/s, which caused the negative pressure at the opposite side of impact (Fig.12(b)) and the skull fracture at the right occipital region of the head. The input force duration (i.e. the length of time that the impact object contacted the head) of this case was counted from the animation of the analysis result, was 3.4 ms.



(a) Simulation outline (b) Intracranial pressure fluctuations ($v = 7 \text{ m/s}$)

Fig. 12. Simulation outline and results of case 9. (a) Simulation outline. The impact velocity (1-15 m/s) was applied to the node that constituted the head model. For better view, only part of the asphalt road model is displayed. (b) The intracranial pressure fluctuations of the impact side and its opposite side. The results show that negative pressure occurred only on the opposite side of impact.

3.3 Relationship between force duration and contusion type

Coup and contrecoup contusions were classified according to the force duration which was obtained from the simulations (Table 3). In coup contusion cases, the input force durations were 1.4~2.7ms, and in contrecoup contusion cases, the input force durations were 2.9~3.7ms. Short (1.4~2.7ms) and long (2.9~3.7ms) force durations were obtained from coup and contrecoup contusion cases, respectively. These results show that when the head is impacted by sharp-cornered objects, coup contusions due to the short force durations are caused more easily; meanwhile, when the head is impacted by objects with flat surfaces, contrecoup contusions due to the long force durations are caused more easily.

	Case	Impact object	Impact region	Force duration
Coup contusion	1	Beer bottle	Frontal region	1.4 ms
	2	Wooden box (1.5 t)	Right temporal region	2.7 ms
	3	Sake bottle (empty: 700 g)	Right parietal region	2.2 ms
Contrecoup contusion	4	Tank lorry	Parietal occipital region	3.7 ms
	5	Steel Box (600 kg)	Occipital region	3.6 ms
	6	Concrete (5.5 m)	Upper side of occipital region	3.7 ms
	7	Wooden deck (10 m)	Occipital region	3.6 ms
	8	Asphalt (160 cm/58 kg)	Occipital region	2.9 ms
	9	Asphalt (156 cm/59 kg)	Right occipital region	3.4 ms

Table 3. Force durations obtained from the simulations. Short (1.4~2.7ms) and long (2.9~3.7ms) force durations were obtained from the coup and contrecoup contusion cases, respectively.

3.4 Summary of chapter 3

In this chapter, the relationship between the input force duration and the dynamic response of the human head were focused by reconstructing the real-world brain injury accident cases using the finite element human head model based on the contusions were caused by the negative pressure inside the skull. The results were shown, in the coup contusion cases, the impact objects were sharp so the short force durations were obtained and the negative pressure occurred at the impact side. In contrast, in the contrecoup contusion cases, the impact objects had flat surfaces so the long force durations were obtained and the negative pressure occurred at the opposite side of impact. In the other words, coup contusion tends to occur when the force duration is shorten, and contrecoup contusion tends to occur when the force duration is lengthen, so the force duration is shown to be the parameter for separating coup or contrecoup contusions.

4. The mechanism of DAI

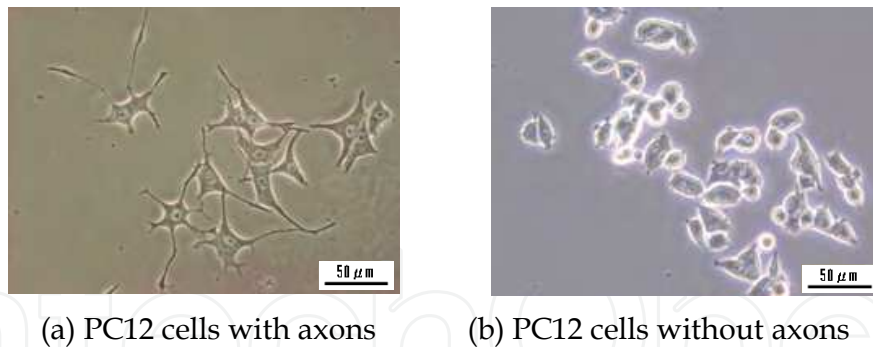
Gennarelli et al. characterized the strain caused by a rotational acceleration load to the head, and proposed the strain threshold of DAI by using finite element models for the crania of human and baboon (Meaney et al., 1995; Susan et al., 1990). They observed the shear deformation generated in each part of the brain with a high speed camera when the head was rotated, and assumed that the strain that caused DAI was larger than 9.4%. Pfister et al. developed a device which could generate shear deformation of cells cultured on a plane by pulling the ground substance and made it possible to produce a strain up to 70% and a strain rate up to 90/s (Pfister et al., 2003). Laplaca et al. cultured cells in a gel and generated 3D deformation of the cells by producing a shear deformation of the gel (strain < 50%, strain rate < 30/s). Neuronal cells showed a lower tolerance to this strain than the glial cells (LaPlaca et al., 2005; Cullen et al., 2007). Tamura et al. analyzed the difference in strain caused by a tensile test between porcine brain tissue and nerve fiber in the white matter, and reported that the maximum neural fiber strain was ~25% of the level in the surrounding tissue (Tamura et al., 2006). Nakayama et al. showed morphological changes of axons and the progress of this damage over time caused by one-dimensional, horizontal oscillations of nerve cells (Nakayama et al., 2001). These data suggested that an axon would receive damage with a strain of larger than 10% and a strain rate of larger than 10/s.

In this chapter, in order to clarify the influence of the axonal damage on the damage of cells, the cytotoxicity and mortality of PC12 cell (rat adrenal pheochromocytoma cell) line were evaluated by applying huge acceleration to cells. Huge acceleration was generated by an impact machine and was given to 2 kinds of cells, i.e. with and without axons.

4.1 Cell culture

In this study, PC12 cell line (obtained from Riken Cell Bank, Tsukuba, Japan) was used. Cells were cultured in DMEM (Dulbecco's Modified Eagle's Medium; Gibco, Gland Island, NY, USA) supplemented with 10% FBS (fetal bovine serum), 10% HS (horse serum), and Penicillin-Streptomycin (10U/ml, 100ng/ml, Sigma-Aldrich, St. Louis, MO, USA) in 95% Air, 5% CO₂ at 37°C.

In the impact experiment, the PC12 cells with and without axons were used. Axons were developed by adding 50ng/ml NGF (nerve growth factor, 2.5S; Invitrogen, Carlsbad, CA, USA). The cells were seeded in PLL (poly-L-lysine)-coated dishes (Φ35mm) at a density of 1×10⁴/cm², and incubated for 5 days. Phase-contrast images of cells are shown in Fig. 13.



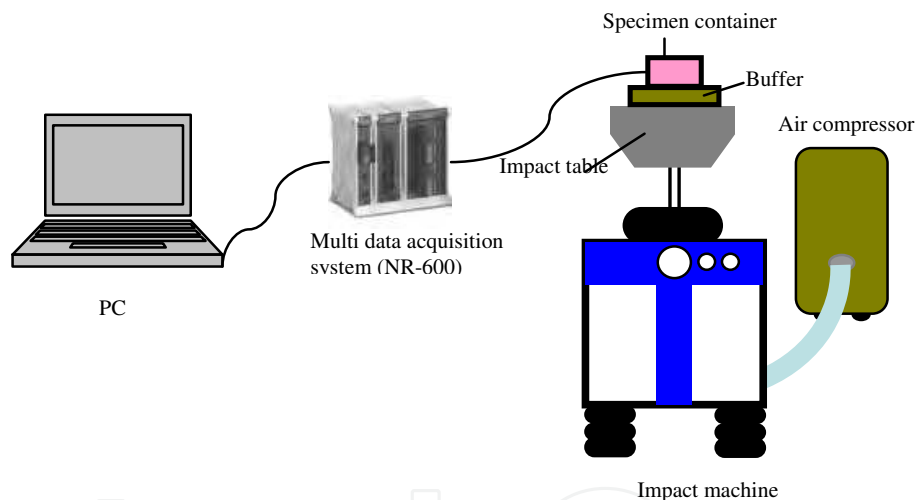
(a) PC12 cells with axons

(b) PC12 cells without axons

Fig. 13. Phase-contrast images of PC12 cells cultured for 5days. (a) PC12 cells with axons. (b) PC12 cells without axons.

4.2 Impact experiment with huge acceleration

The outline of the impact experiment is shown in Fig. 14. The impact experiments were carried out with an SM-100-3P impact machine (AVEX Electronics Inc., PA, USA). The impact machine can accelerate the specimen, with a range of acceleration of 3~20000 G and for duration of 0.1~60ms.



(a) Devices used for the impact experiments



(b) Impact machine (c) Cultured dish and culture solution (d) Specimen container (e) Impact table

Fig. 14. Major components of the impact experiment. A dish seeded with PC12 cells was filled with culture solution (c), and fixed in position in a stainless plate (d). The plate was then fixed on the impact table (e). The impact table was elevated and dropped by the compressor.

A dish seeded with PC12 cells was filled with culture solution (Fig. 14(c)), and fixed in position in a stainless plate (Fig. 14(d)). The plate was then fixed on the impact table (Fig. 14(e)). The impact table was elevated and dropped by the compressor. The impact table collided against the buffer generating an impact with huge velocity to the dish.

The strain applied to the cultured dish was measured with a strain gauge (KFG-2N-120-C1; Kyowa Electronic Instruments Co.), which was attached to the bottom of the dish and connected to a multi-data acquisition system (NR-600; Keyence Co.). A total of 72 impact experiments were carried out, i.e. 6 experiments per condition. The input acceleration ranged from 3000 G to 10000 G, and the duration of all accelerations was 0.1ms.

4.3 Evaluation of Injury

4.3.1 Cytotoxicity of PC12 Cells

Cytotoxicity of cells was measured by the LDH (lactate dehydrogenase) assay. LDH is a soluble cytosolic enzyme that is released into the culture medium following loss of membrane integrity resulting from either apoptosis or necrosis.

After the impact, the culture solution in the dish was centrifuged for 10 minutes at 250 G, 100 μ l of the reaction solution (cytotoxicity detection kit (LDH), Roche Diagnostics) was added to 100 μ l of the supernatant. The reactions were incubated at room temperature for 30 min using 96-well plates (96-well Micro Test III assay Plate, BD Falcon), and 1N-HCl was added as a stop solution. The absorbance of each specimen was measured at 490 nm by a Microplate Reader (Model 680; Bio-Rad Laboratories). Similarly, the absorbance of the low control specimens (no load cells) and high control specimens (cells dissolved by 1% TritonX-100 in PBS) were measured. The cytotoxicity of PC12 cells was calculated by the following equation.

$$\text{Cytotoxicity (\%)} = (C - LC) / HC \times 100\% \quad (1)$$

where C is the LDH quantity (IU/l) obtained from the impact experiment specimen, LC is the LDH quantity (IU/l) obtained from the low control specimen, and HC is the LDH quantity (IU/l) obtained from the high control specimen.

4.3.2 Mortality of PC12 cells

Mortality of cells was measured by the dye exclusion method with trypan blue dye. This method determines cell viability by mixing a suspension of live cells with a dilute solution of trypan blue; cells that exclude dye are considered to be alive, while stained cells are considered to be dead.

After the impact, cells were separated from the dish with 0.25% Trypsin-EDTA (Gibco), collected in a microcentrifuge tube (1.5 ml), and centrifuged for 30 seconds at 2000 G.

$$\text{Mortality (\%)} = N / M \times 100\% \quad (2)$$

where N is the number of the dead cells and M is the total number of cells.

4.3.3 Morphological change of axon

When an axon is damaged, terminal swellings coincide with the detachment of the growth cones from the substrate. The detachment of the growth cones from the substrate destroys the cytoskeletal network, which determines and maintains cell shape, resulting in a spherical deformation of the axon. Terminal swellings form in the early stages of the injury. When the cytoskeletal destruction occurs at non-terminal sites along the axon, spherical deformations develop slowly, and these appear as beads. Beadings grow in the later stages of injury (Nakayama et al., 2001; Fujiwara et al., 2004).

After the impact, the morphological changes of the axons were observed with a phase-contrast microscope.

4.3.4 Statistical analysis

Statistical analysis of the cytotoxicity and mortality of cells with axons and without axons for each experimental condition were assessed with the t-test; $p < 0.05$ was considered to be statistically significant. Data were expressed as the mean \pm standard error of the mean (SEM).

4.4 Results of damage evaluation

4.4.1 Strain and strain rate obtained from the impact experiments

The average strain and strain rate at the bottom of dish are shown in Table 4. As an example, the strain fluctuation when the peak of acceleration was 7000G is shown in Fig.15.

A strain from 0.035% to 0.201% and a strain rate from 6.67/s to 19.02/s were measurable on the bottom of dish with the input accelerations from 3000 G to 10000 G. The strain measured at the bottom of dish had increased linearly as the input acceleration increased.

The strain rate tended to increase linearly as the input acceleration increased. However, when the input acceleration was 5000, 6000 and 8000 G, the strain rate was 13.02/s, 13.11/s, and 13.36/s, respectively. There was no significant difference between these strain rates. The strain rate obtained at 7000 G was 14.62/s, which was larger than the strain rate obtained at 8000G. It was difficult to control the duration of the acceleration accurately in the impact experiment when the input acceleration was very powerful. Although the strain obtained at 8000 G was larger than the strain obtained at 7000G, the duration of 8000 G became longer than the duration of 7000 G, resulting in the smaller strain rate at 8000 G.

Condition number	Peak acceleration [G]	Duration [ms]	Average strain [%]	Average strain rate (1/s)
1	3000	0.1	0.035	6.67
2	5000	0.1	0.065	13.02
3	6000	0.1	0.148	13.11
4	7000	0.1	0.164	14.62
5	8000	0.1	0.187	13.36
6	10000	0.1	0.201	19.02

Table 4. Strain and strain rates obtained from the impact experiments. The strain rate tended to increase linearly as the input acceleration increased.

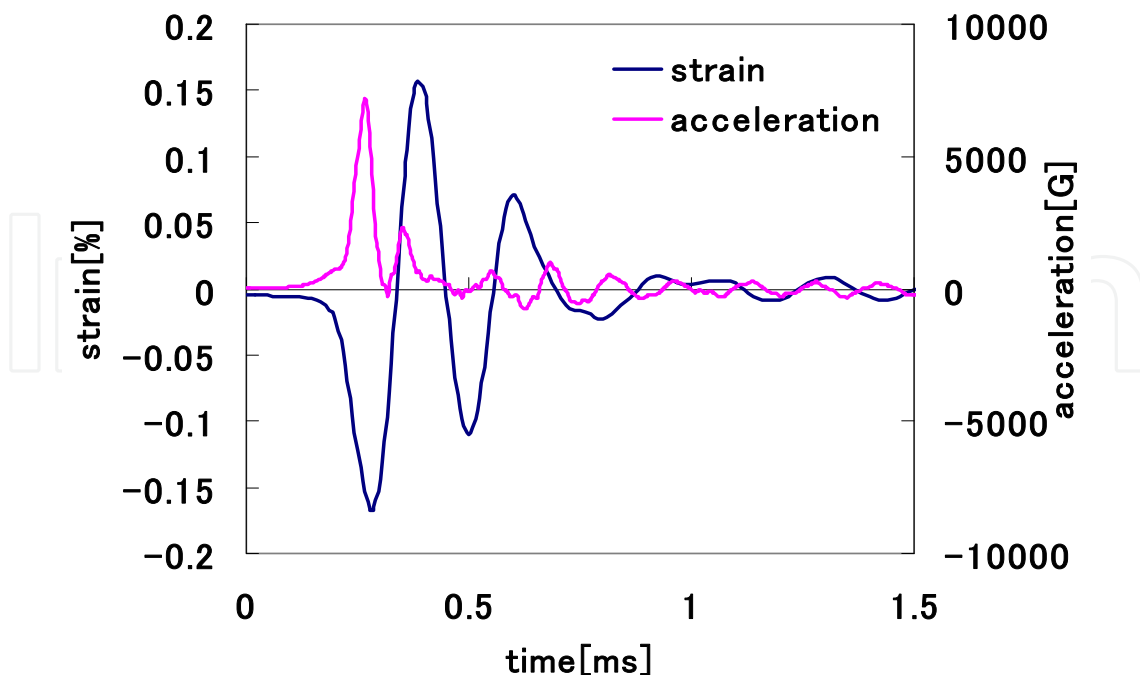


Fig. 15. Strain fluctuation when the peak of the acceleration was 7000 G. The strain of this input was 0.164%.

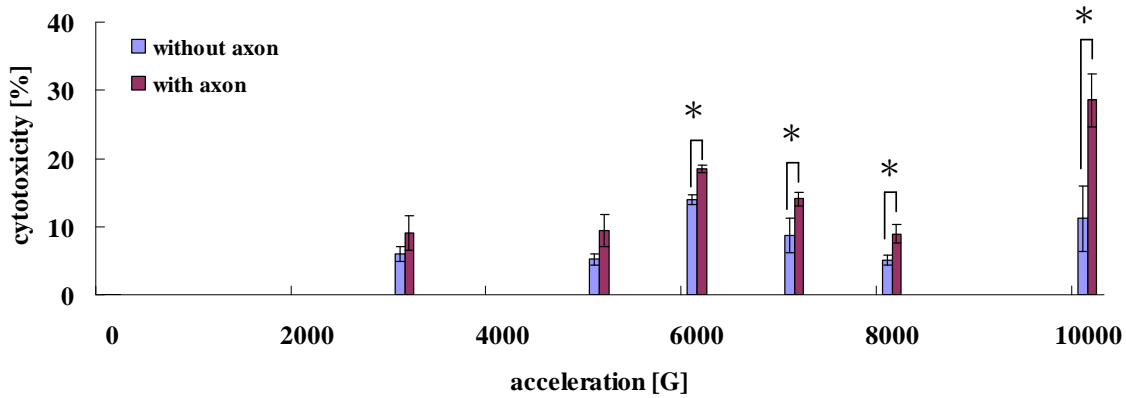
4.4.2 Cytotoxicity of PC12 cells

Cytotoxicity of cells with and without axons immediately after the impact experiment is shown in Fig.16. The relationship between the input acceleration and cytotoxicity of cells is shown in Fig.16 (a), the relationship between the strain and cytotoxicity of cells is shown in Fig.16 (b), and the relationship between the strain rate and cytotoxicity of cells is shown in Fig.16(c). Since the input of the impact experiment was acceleration, the strain rate could not be controlled in detail; the data obtained from 5000-8000G were concentrated on around 14/s as shown in Table 4.

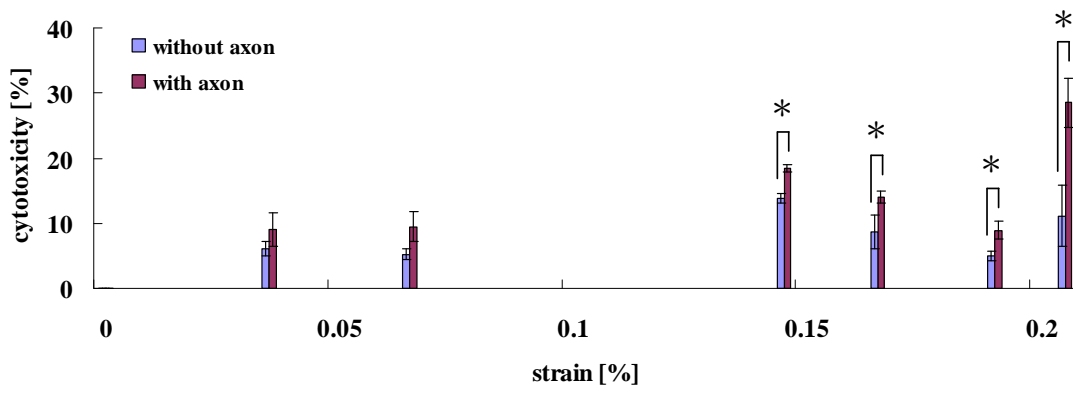
Cytotoxicity of cells seemed to increase as the input acceleration and strain increased, but these relationships did not show strong correlations (Figs. 16(a), and 16(b)). Although the tendency that cytotoxicity of cells increased as the strain rate increased was shown, the correlation could not be quantitatively evaluated, because in the small strain rate range around 14/s cytotoxicity of cells did not increase monotonically.

For the two results obtained from 3000 and 5000 G (correspond to 0.035% and 0.065% in the strain, and to 6.67/s and 13.02/s in the strain rate), cytotoxicity of cells with axons was not significantly higher than in cells without axons. When the input acceleration was larger than 6000G, the strain was larger than 0.15%, and the strain rate was larger than 13.11/s, cytotoxicity of cells with axons was significantly higher than in cells without axons (Figs. 16(a), 16(b), and 16(c); * $p < 0.05$).

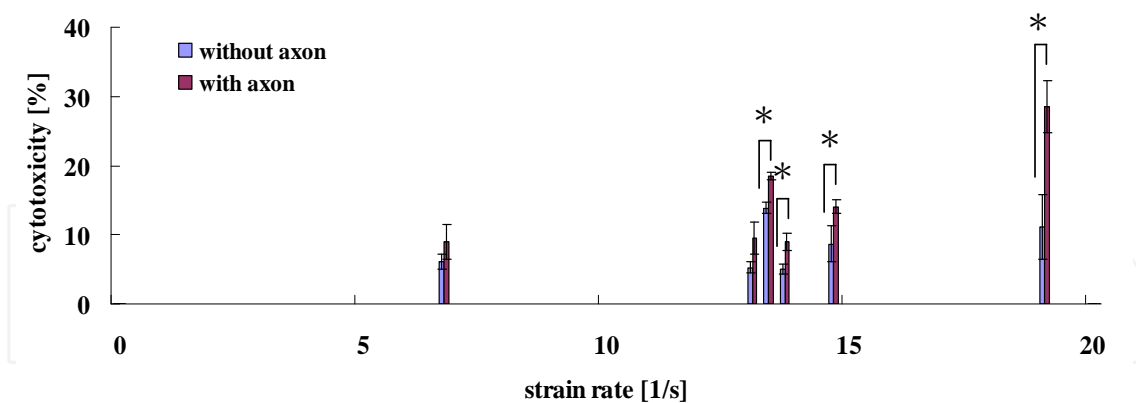
Therefore, it appeared that cytotoxicity of cells increased as the strain rate increased, and cells with axons were more easily damaged than cells without axons when the strain rate was larger than 13.11/s.



(a) Relationship between the input acceleration and cytotoxicity of PC12 cells



(b) Relationship between the strain and cytotoxicity of PC12 cells



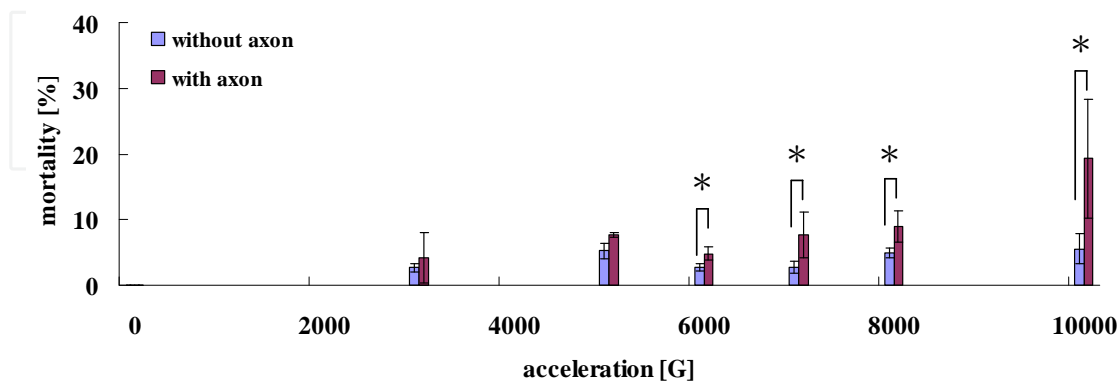
(c) Relationship between the strain rate and cytotoxicity of PC12 cells

Fig. 16. Experimental results of cytotoxicity of PC12 cells. Error bars represent SEM. (* $p < 0.05$)

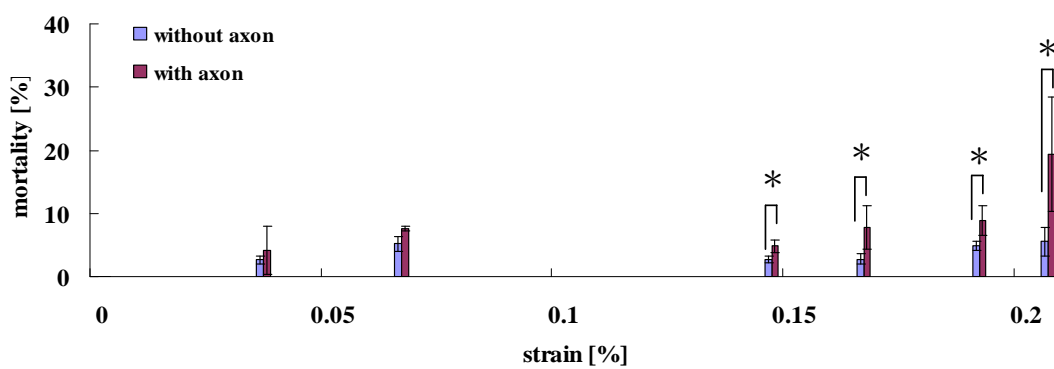
4.4.3 Mortality of PC12 cells

Mortality of cells with and without axons immediately after the impact experiment is shown in Fig. 17. The relationship between the input acceleration and mortality of cells is shown in Fig. 17(a), the relationship between the strain and mortality of cells is shown in Fig. 17(b), and the relationship between the strain rate and mortality of cells is shown in Fig. 17(c).

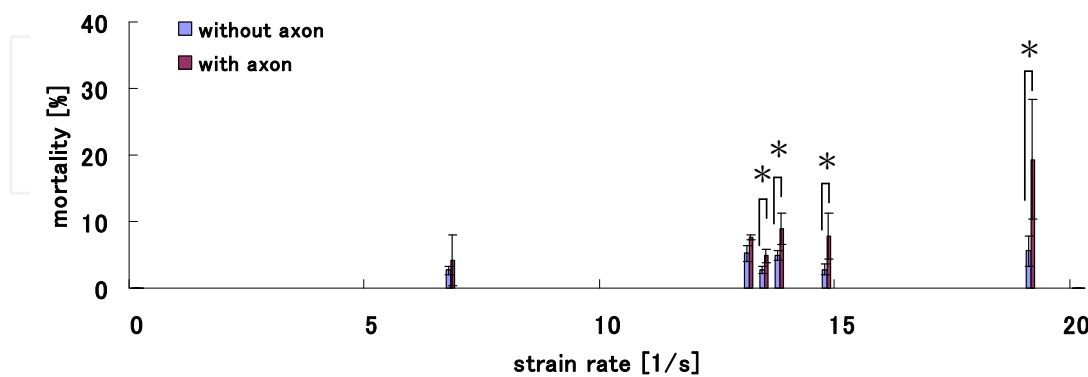
Mortality of cells seemed to increase as the input acceleration and strain increased, but these relationships did not show strong correlations (Fig. 17(a), and 17(b)). Although the tendency that mortality of cells increased as the strain rate increased was shown, the correlation could not be quantitatively evaluated, because in the small strain rate range around 14/s mortality of cells did not increase monotonically.



(a) Relationship between the input acceleration and mortality of PC12 cells



(b) Relationship between the strain and mortality of PC12 cells



(c) Relationship between the strain rate and mortality of PC12 cells

Fig. 17. Experimental result of mortality of PC12 cells · Error bars represent SEM. (* $p < 0.05$)

For the two results obtained from 3000 and 5000 G (correspond to 0.035% and 0.065% in the strain, and to 6.67/s and 13.02/s in the strain rate), mortality of cells with axons was not

significantly higher than in cells without axons. When the input acceleration was larger than 6000 G, the strain was larger than 0.15%, and the strain rate was larger than 13.11/s, mortality of cells with axons was significantly higher than in cells without axons (Figs. 17(a), 17(b), and 17(c); $*p < 0.05$).

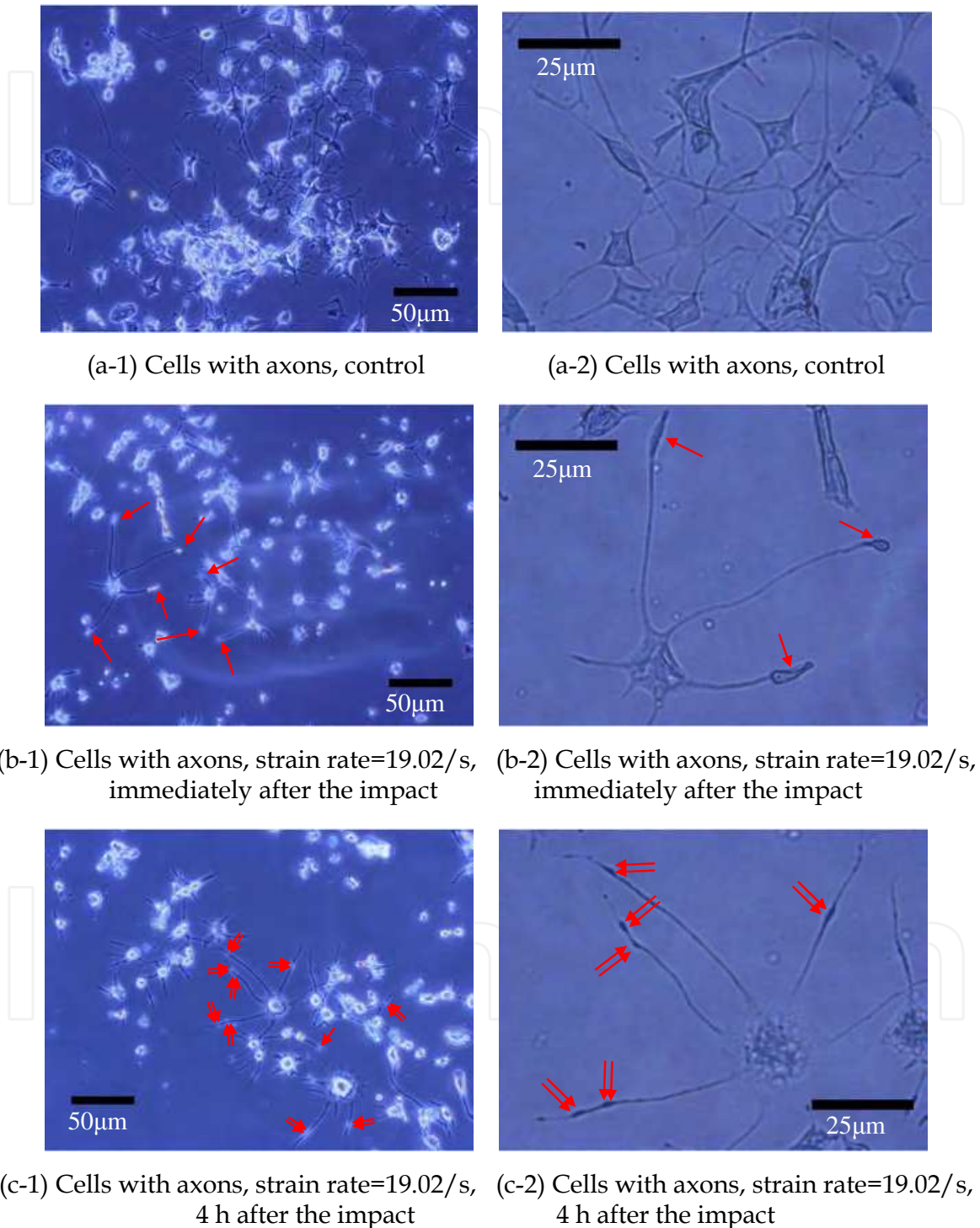


Fig. 18. Phase-contrast images of PC12 cells, control (a-1, a-2), immediately after the impact (b-1, b-2) and 4 h after the impact (c-1, c-2). For a clearer view, (a-1), (b-1), and (c-1) are enlarged in (a-2), (b-2), and (c-2), respectively. Terminal swellings are indicated with single arrows and beadings are indicated with double arrows.

Therefore, it appeared that mortality of cells increased as the strain rate increased, and cells with axons had an increased mortality than cells without axons when the strain rate was larger than 13.11/s.

4.4.4 Morphological change

In order to observe damage to axons, cells with axons were observed with a phase-contrast microscope. Phase-contrast images of cells with axons on the dish are shown in Fig.18.

Phase-contrast images of cells with axons before the experiments (control) are shown in Figs. 18(a-1) and 18(a-2). Cells extending their axons and a network creates with these axons can be observed. Cells and their axons attached to the substrate. Terminal swellings or the beadings of axons are not observed at this stage. Phase-contrast images of cells immediately after the impact with the strain rate of 19.02/s are shown in Figs. 18(b-1) and 18(b-2); terminal swellings of axons are indicated with single arrows in the figures. Terminal swellings can be observed when the terminals of axons detach from the substrate. Since beading occurs in the later stages of damage, beading can not be observed yet at this stage. Phase-contrast images of cells 4 h after the impact with the strain rate of 19.02/s are shown in Figs. 18(c-1) and 18(c-2); beadings in the damaged regions are indicated with double arrows in the figures. Although beadings can not be observed in the images immediately after the impact as shown in Figs. 18(b-1) and 18(b-2), beadings can be clearly observed in the images taken after 4 h as shown in Figs. 18(c-1) and 18(c-2).

4.5 Summary of chapter 4

In this chapter, in order to study the influence of the axonal damage on cell damage, an impact experiment with huge acceleration was performed on PC12 cell line. In order to evaluate damage to axon, the impact experiments were performed on cells with and without axons. The strain at the bottom of cultured dish was measured, and the strain rate was calculated. The cytotoxicity and mortality of PC12 cells were evaluated by the input acceleration, strain and strain rate. As a result, the strain rate seemed to be the most appropriate to evaluate the cytotoxicity and mortality of cells. The cytotoxicity and mortality of cells increased as the strain rate increased, and cells with axons were more easily damaged and had an increased mortality than cells without axons when the strain rate was larger than 13.11/s. These data suggest that the presence of axons increased the cytotoxicity and mortality of cells.

5. Conclusion

In this study, to elucidate the mechanics of head injuries, the engineering approach using finite element analysis and the biological approach using cultured cells are performed. In the engineering approach, the results of the reconstruction of the real-world brain injury accident cases are shown, in the coup contusion cases, the negative pressure occurred at the impact side and it had direct correlation with the short force durations. In contrast, in the contrecoup contusion cases, the negative pressure occurred at the opposite side of impact and it had direct correlation with the long force durations. As the result, the force duration is shown to be the parameter for separating coup or contrecoup contusions. In the biological approach, the results of the impact experiments using the cultured cells are shown, the strain rate seemed to be the most appropriate to evaluate the cytotoxicity and mortality of cells. Damage to axons was confirmed by terminal swellings and beadings of the axons. These data indicated that the presence of axons increased the cytotoxicity and mortality of cells.

6. Future directions

In the future works, in order to evaluate all types of traumatic brain injury comprehensively, the tolerance of nerve damage which is obtained from the impact experiment of cultured cells is applied to numerical analysis. Therefore, to construct a human head finite element model containing the nerve fibers, a method to accurately measure the material properties of nerve fibers have to be developed and the structure of the neural network inside the skull have to be clarified by the image processing.

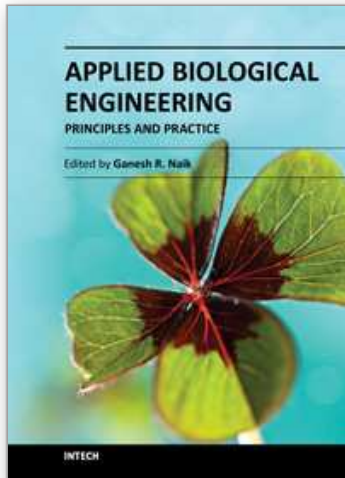
7. Acknowledgement

We thank Associate Prof. Atsushi Senoo (Tokyo Metropolitan University, Faculty of Health Sciences, Division of Radiological Sciences) for his assistance in photographing MRI data to construct the finite element human head model.

8. References

- Aomura, S.; Fujiwara, S & Ikoma, T. (2002). The Study on the Influence of Different Interface Conditions on the Response of Finite Element Human Head Models under Occipital Impact Loading, *JSME International Journal, Series C*, Vol.46, No.2, pp.583-593.
- Aomura, S.; Zhang, Y.; Fujiwara, S. & Nishimura, A. (2008). Dynamic Analysis of Cerebral Contusion under Impact Loading, *Journal of Biomechanical Science and Engineering*, Vol. 3, No. 4, pp.499-509.
- Cullen D.K.; Simon C.M. & LaPlaca M.C. (2007). Strain rate-dependent induction of reactive astrogliosis and cell death in three-dimensional neuronal-astrocytic co-cultures, *Brain Research*, Vol.1158, pp.103-115.
- Doorly, M.C. & Gilchrist, M.D. (2006). The Use of Accident Reconstruction for the Analysis of Traumatic Brain Injury Due to Head Impacts Arising from Falls, *Computer Methods in Biomechanics and Biomedical Engineering*, Vol.9, No.6, pp.371-377.
- Fujiwara S.; Ogawa Y.; Hirabayashi M.; Inamura K. & Aihara H. (1998). Biomechanics of Cerebral Contusion and Diffuse Axonal Injury, *Proceedings of the 6th Indo Pacific Congress on Legal Medicine and Forensic Sciences*, pp.1003-1006.
- Fujiwara S.; Yanagisawa A.; Sato H.; Shindo Y.; Koide K. & Nishimura A. (2004). DAI Diagnosis Using β -APP mRNA Expression Analysis and its Application to Forensic Medicine, *Research and Practice in Forensic Medicine*, Vol.47, pp.85-90.
- Fujiwara, S.; Yanagida, Y. & Mizoi, Y. (1989). Impact Induced Intra-cranial Pressure Caused by an Accelerated Motion of the Head or by Skull Deformation: An Experimental Study Using Physical Models of the Head and Neck, and Ones of the Skull, *Forensic Science International*, Vol.43, pp.159-169.
- Fujiwara, S.; Yanagida, Y.; Fukunaga, T.; Mizoi, Y. & Tatsuno, Y. (1986). Studies on Cerebral Contusion in the Fatal Cases by Blow, Fall and Fall Down, *The Japanese Journal of Legal Medicine*, Vol.40, No.4, pp.377-383.
- Gennarelli, T.A. (1983). Head Injury in Man and Experimental Animals: Clinical Aspects, *Acta Neurochirurgica*, Suppl.32, pp.1-32.
- Gross, A.G. (1958). A New Theory on the Dynamics of Brain Concussion and Brain Injury, *Journal of Neurosurgery*, Vol.15, pp.548-561.
- Gurdjian, E.S.; Lissner, H.R.; & Hodson, V.R. (1966). Mechanism of Head Injury, *Clinical Neurosurgery*, Vol.12, pp.112-128.

- LaPlaca M.C.; Cullen D.K.; McLoughlin J.J. & Cargill R.S. (2005). High rate shear strain of three-dimensional neural cell cultures: a new in vitro traumatic brain injury model, *Journal of Biomechanics*, Vol.38, No.5, pp.1093-1105.
- Meaney D.F.; Smith D.H.; Shreiber D.I.; Bain A.C.; Miller R.T.; Ross D.T. & Gennarelli T.A. (1995). Biomechanical Analysis of Experimental Diffuse Axonal Injury, *Journal of Neurotrauma*, Vol.12, No.4, pp.689-694.
- Nahum, A.M. & Smith, R. (1977), Intracranial Pressure Dynamics during Head Impact, *Proceeding of 21st Stapp car Crash Conference*, pp.339-366.
- Nakayama Y.; Aoki Y. & Niitsu H. (2001). Studies on the mechanisms responsible for the formation of focal swellings on neuronal processes using a novel in vitro model of axonal injury, *Journal of Neurotrauma*, Vol.18, No.5, pp.545-554.
- Nishimoto, T.; Murakami, S.; Abe, T. & Ono, K. (1998). Mechanical Properties of Human Cranium and Effect of Cranial on Extradural Hematoma, *Transactions of the Japan Society of Mechanical Engineers, Part A*, Vol.61, No.591, pp. 2386-2392.
- Ommaya A.K. & Gennarelli T.A. (1974). Cerebral concussion and traumatic unconsciousness, correlation of experimental and clinical observations on blunt head injuries, *Brain*, Vol.97, pp.633-654.
- Pfister B.J.; Weihs T.P.; Betenbaugh M. & Bao G. (2003). An in vitro Uniaxial Stretch Model for Axonal Injury, *Annals of Biomedical Engineering*, Vol.31, No.5, pp.589-598.
- Raul, J.S.; Baumgartner, D.; Willinger, R. & Ludes, B. (2006). Finite Element Modelling of Human Head Injuries Caused by a Fall, *International Journal of Legal Medicine*, Vol.120, No.4, pp.212-218.
- Riordain, K.O.; Thomas, P.M.; Phillips, J.P. & Gilchrist, M.D. (2003). Reconstruction of Real World Head Injury Accidents Resulting from Falls using Multibody Dynamics, *Clinical Biomechanics*, Vol.18, pp.590-600.
- Susan S.M.; Lawrence E.T. & Thomas G. (1990). Physical Model Simulation of Brain Injury in the Primate, *Journal of Biomechanics*, Vol.23, No.8, pp.823-836.
- Tamura A.; Nagayama K. & Matsumoto T. (2006). Measurement of Nerve Fiber Strain in Brain Tissue Subjected to Uniaxial Stretch (Comparison Between Local Strain of Nerve Fiber and Global Strain of Brain Tissue), *Journal of Biomechanical Science and Engineering*, Vol.1, No.2, pp.304-315.
- Viano, D.C.; Casson, I.R.; Pellman, E.J.; Zhang, L.; King, A.I. & Yang, K.H. (1998). Concussion in Professional Football Brain Responses by Finite Element Analysis: Part 9, *Neurosurgery*, Vol.57, No.5, pp.891-916.
- Willinger, R. & Baumgartner, D. (2003). Human Head Tolerance Limits to Specific Injury Mechanisms, *International Journal of Crashworthiness*, Vol.6, No.8, pp.605-617.
- Yanagida, Y.; Fujiwara, S. & Mizoi, Y. (1989). Differences in the Intra-cranial Pressure Caused by a 'Blow' and/or a 'Fall' – An Experimental Study Using Physical Models of the Head and Neck, *Forensic Science International*, Vol.41, pp.135-145.
- Zhang, L.; Hardy, W.N.; Omori, K.; Yang, K.H.; & King, A.I. (2001). Recent Advances in Cerebral Injury Research: A New Model and New Experimental Data, *Proceedings of the ASME Bioengineering Conference*, pp.831-832.
- Zhang, Y.; Aomura, S.; Nakadate, H. & Fujiwara, S. (2010). Study on the Mechanism of Cerebral Contusion Based on Judicial Autopsy Report, *Proceedings of the 6th World Congress on Biomechanics*, Vol.31, pp.505-508.



Applied Biological Engineering - Principles and Practice

Edited by Dr. Ganesh R. Naik

ISBN 978-953-51-0412-4

Hard cover, 662 pages

Publisher InTech

Published online 23, March, 2012

Published in print edition March, 2012

Biological engineering is a field of engineering in which the emphasis is on life and life-sustaining systems. Biological engineering is an emerging discipline that encompasses engineering theory and practice connected to and derived from the science of biology. The most important trend in biological engineering is the dynamic range of scales at which biotechnology is now able to integrate with biological processes. An explosion in micro/nanoscale technology is allowing the manufacture of nanoparticles for drug delivery into cells, miniaturized implantable microsensors for medical diagnostics, and micro-engineered robots for on-board tissue repairs. This book aims to provide an updated overview of the recent developments in biological engineering from diverse aspects and various applications in clinical and experimental research.

How to reference

In order to correctly reference this scholarly work, feel free to copy and paste the following:

Yuelin Zhang, Shigeru Aomura, Hiromichi Nakadate and Satoshi Fujiwara (2012). Study on the Mechanism of Traumatic Brain Injury, Applied Biological Engineering - Principles and Practice, Dr. Ganesh R. Naik (Ed.), ISBN: 978-953-51-0412-4, InTech, Available from: <http://www.intechopen.com/books/applied-biological-engineering-principles-and-practice/study-on-the-mechanism-of-traumatic-brain-injury->

INTECH
open science | open minds

InTech Europe

University Campus STeP Ri
Slavka Krautzeka 83/A
51000 Rijeka, Croatia
Phone: +385 (51) 770 447
Fax: +385 (51) 686 166
www.intechopen.com

InTech China

Unit 405, Office Block, Hotel Equatorial Shanghai
No.65, Yan An Road (West), Shanghai, 200040, China
中国上海市延安西路65号上海国际贵都大饭店办公楼405单元
Phone: +86-21-62489820
Fax: +86-21-62489821

© 2012 The Author(s). Licensee IntechOpen. This is an open access article distributed under the terms of the [Creative Commons Attribution 3.0 License](#), which permits unrestricted use, distribution, and reproduction in any medium, provided the original work is properly cited.

IntechOpen

IntechOpen